3D RECONSTRUCTION OF CORONARY ARTERIES FROM ROTATIONAL X-RAY ANGIOGRAPHY

Ruben Cardenes[1] *Alexey Novikov*[1] *Julian Gunn*[2] *Rod Hose*[2] *Alejandro F. Frangi*[1,2]

[1] Center for Computational Imaging & Simulation Technologies in Biomedicine (CISTIB) – Universitat Pompeu Fabra and CIBER-BBN, Barcelona, Spain
[2] University of Sheffield, Sheffield, U.K.

ABSTRACT

This paper presents a 3D reconstruction method of coronary arteries from multiple projections, that works efficiently in two steps: first, a 2D processing is performed to obtain and classify the vessels branches on the projections, estimating also the radii. Then, a novel 3D reconstruction step is performed from pair of projections, finding the best intersections between ray bundles corresponding to the same branches to extract the 3D vessel trajectories, that is robust to motion. Topological constraints are included implicitly imposing vessel connectivity and tubular construction. The preliminary results presented here from a digital phantom and from real data, show good accuracy and performance of the method.

Index Terms— 3D reconstruction, coronary arteries, projections, X-ray angiography, 3DCA, skeletons

1. INTRODUCTION

Assessment of coronary artery disease (CAD) is usually carried out by Conventional Coronary Angiography (CCA) or Computer Tomography Angiography (CTA), imaging [1], especially multi-detector CT (MDCT), that provides high image quality overcoming 2D limitations of CCA such as vessel overlapping and foreshortening. However, rotational X-ray angiography or 3DCA can solve some of the disadvantages of CCA, and compete with MDCT, with the use of motion compensated reconstruction techniques. Additionally, 3DCA can be acquired in the operation room, before and after treatment, and still provides higher spatial resolution, making it an extremely useful image modality to analyze coronary arteries. The main problem in 3DCA is how to combine the information of several projections compensating the cardiac and respiratory motion, in order to construct a valid vascular model. Additionally, there are some other problems, such as intensity inhomogeneity, vessel foreshortening and overlap of different structures such as the catheter, bones or diaphragm, making this reconstruction a very challenging problem.

First author funded by Beatriu de Pinos program, AGAUR, Generalitat de Catalunya. Work partially funded by CDTI CENIT-cvREMOD grant, Spain.

Several techniques have been proposed for this particular application. In [2], the reconstruction is performed computing the 2D vessel centerlines from the projections, and searching correspondences in them, to then obtain a 4D field representing the motion, without using the ECG signal. In [3], the background of the projections is removed using a top hat filter, and then, a thresholded Algebraic Reconstruction Technique (ART) method of [4] is used for ECG gated projections. In [5] a back-projection of the projections' vesselness into a 3D volume is performed, using all the possible pairs of projections of the same ECG time step.Then, the 3D volume is segmented using fast marching, to finally do a backtracking to obtain the skeleton of the coronaries. In [6] reconstruction is done by an optimization scheme from two uncalibrated angiographic images with 14 parameters involved, where two errors are minimized, distances and direction vectors of corresponding skeleton points in the original projections and in reconstructed skeleton projections. The correspondence of centerline points between the two projections is carried out using epipolar constraints.

The approach presented here has similar characteristics to the works mentioned above. The method proceeds in two steps: 2D angiographic processing plus a 3D reconstruction stage, as in [2, 3, 5, 6]. However, there is no need here to generate an initial reconstruction from the projections, as carried out in [3] and [5], and the novelty of this method is a 3D strategy to obtain the 3D centerlines of the coronaries, using 2D branches correspondences of the 2D skeletons, not point to point as done in [2, 6] . This 3D process is novel, robust, and is able to account for cardiac and respiratory motion. In this paper we will focus in the 3D processing stage.

2. METHOD

The two stages proposed are: first, a 2D processing of the projections to identify consistently the arteries' branches, to classify them across the entire sequence, and to compute the vessel radii. Then, a 3D step is performed to obtain 3D models at different time steps.

2.1. 2D projections processing

Given the complexity of this step, it will be outlined very briefly here. The full description will be presented in a separate work, and this paper will be focused on the 3D processing stage. This 2D pipeline starts with a multi-scale vesselness filtering [7] to obtain the main vessel structures. Then, a 2D ridge extraction is carried out on the vesselness images to find the curves representing the main vessels. This processing provides a disconnected set of segments that will be reconnected in the next step using a fast marching approach. The resulting structure still needs some further processing, especially topological corrections, such as removal of non plausible segments, inclusion of missing branches, and removal of other structures (catheter, diaphragm and bones). Finally, the branches are labeled on each projection using a strategy exploiting the spatial coherence existing across the image sequence.

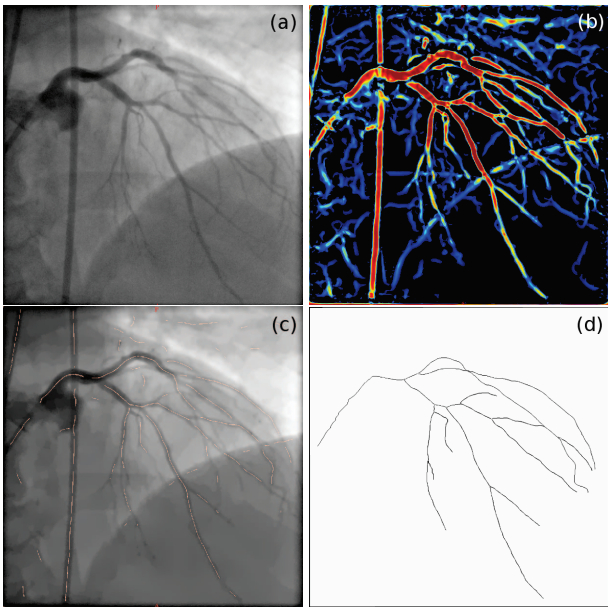


Fig. 1. 2D processing steps: (a) 2D angiographic projection, (b) color-coded vesselness function, (c) extracted ridges, and (d) cleaned connected components of the coronary tree.

2.2. 3D branch reconstruction from two projections

From the labeled 2D skeletons, the 3D structure of the vascular tree can be extracted. In our case, the reconstruction is done on pair of projections. Let's denote $\mathcal{P}_n$ to projection n, and $\mathbf{p}_{n,j}$ to the centerline points lying on $\mathcal{P}_n$ for the j^{th} branch. Here, branch is any segment between two bifurcations, or between one bifurcation and one end point. Notice that from the previous step, the branches correspondences between any two projections n and m are already known: $L(\mathbf{p}_{n,j}) = L(\mathbf{p}_{m,j}) = j, \ \forall\, n, m \in \{1, ..., N_p\}$, where $L(\mathbf{p})$ is the branch label corresponding to a point $\mathbf{p}$, and N_p the number of projections. Then, let's denote $\mathbf{R}_{n,j}$, to the set of rays (ray bundle) joining all branch points $\mathbf{p}_{n,j}$, to the focal point $\mathbf{f}_n$, and $\mathbf{R}^i_{n,j}$ each of the i^{th} individual rays,

$$\mathbf{R}^i_{n,j} = \overline{\mathbf{p}^i_{n,j}\mathbf{f}_n} \qquad \forall\, i \in \{1, ..., l_{n,j}\},$$

where $\mathbf{p}^i_{n,j}$ is the i^{th} point of branch j at projection n, and $l_{n,j}$ is the length of branch j at projection n, see Fig. 2. Assuming exact matching, from two projections corresponding to the same cardiac phase, $\mathcal{P}_n, \mathcal{P}_m$, the problem of finding the 3D coordinates of the points of branch j, $\mathbf{q}_j$, is reduced to find the intersection points of the two set of rays:

$$\mathbf{q}_j = \mathbf{R}_{n,j} \cap \mathbf{R}_{m,j}.$$

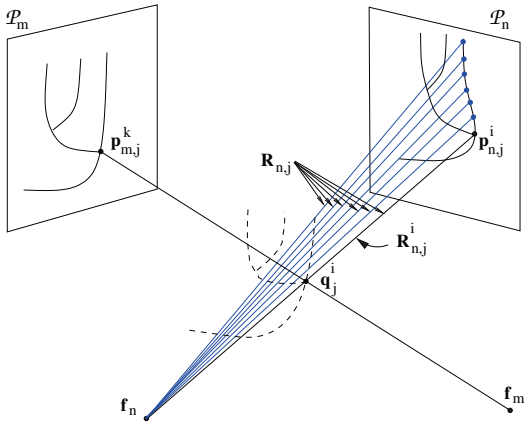


Fig. 2. Schematic view of two projections, correspondence of point $\mathbf{q}^i_j$ in the two projections, and rays generated from one of the branches in one projection.

However, there is no exact matching due to respiratory motion and other phenomena, such as non exact ECG gating (corresponding projections are not necessarily at exactly the same cardiac phase). Therefore, an estimation of the branches positions in 3D has to be performed. The solution proposed here for a single branch is to obtain the closest points on the ray bundle $\mathbf{R}_{n,j}$, with respect to the ray bundle $\mathbf{R}_{m,j}$, with $\mathcal{P}_n$ and $\mathcal{P}_m$ at the same cardiac phase, chosen from the ECG signal, as shown in Fig. 3. We will consider the projection $\mathcal{P}_n$ as the *master projection* and $\mathcal{P}_m$, the *guiding projection*, that is used to estimate the 3D position of the branch points on the rays traced by the *master* one. More specifically, the 3D points of branch j are obtained as this:

$$\mathbf{q}^i_j = \underset{\mathbf{x}}{argmin}\{d(\mathbf{x}, \mathbf{R}^k_{m,j}) \ \mid \ \mathbf{x} \in \mathbf{R}^i_{n,j}\},$$

where i is the ray index on $\mathbf{R}_{n,j}$ and k is the corresponding index on $\mathbf{R}_{m,j}$. This correspondence means that if both ray bundles have the same size, then $k = i$, but in the general case of different size bundles:

$$k = i \cdot l_{m,j}/l_{n,j}.$$

The distance $d(\mathbf{x}, \mathbf{R}^k_{m,j})$ is the minimum Euclidean distance between $\mathbf{R}^i_{n,j}$ and $\mathbf{R}^k_{m,j}$. Expressing them in parametric form:

$$\mathbf{R}^i_{u,j}(s) = \mathbf{f}_u + s \cdot (\mathbf{p}^i_{u,j} - \mathbf{f}_u) = \mathbf{f}_u + s \cdot \mathbf{v}^i_{u,j},\ u = \{n, m\}$$

then, the minimum distance between them is given by

$$d = |\mathbf{n} \cdot \mathbf{w}|,$$

where $\mathbf{n}$ is the normalized cross product of the ray directors vectors: $\mathbf{n} = (\mathbf{v}^i_{n,j} \times \mathbf{v}^i_{m,j})/|\mathbf{v}^i_{n,j} \times \mathbf{v}^i_{m,j}|$, and $\mathbf{w}$ any vector joining the two lines, for instance, $\mathbf{w} = \mathbf{f}_m - \mathbf{f}_n$. Then, the closest point on ray $\mathbf{R}^i_{n,j}$ to the ray $\mathbf{R}^k_{m,j}$ can be computed as $\mathbf{x} = \mathbf{f}_n + t\mathbf{v}^i_{n,j}$, where

$$t = (a_{22}(\mathbf{v}^i_{n,j} \cdot \mathbf{w}) - a_{12}(\mathbf{v}^i_{m,j} \cdot \mathbf{w}))/|\mathcal{A}|,$$

and a_{ij} are the components of matrix $\mathcal{A}$:

$$\mathcal{A} = \begin{pmatrix} \mathbf{v}^i_{n,j}\mathbf{v}^i_{n,j} & -\mathbf{v}^i_{m,j}\mathbf{v}^i_{n,j} \\ \mathbf{v}^i_{n,j}\mathbf{v}^i_{m,j} & -\mathbf{v}^i_{m,j}\mathbf{v}^i_{m,j} \end{pmatrix}$$

2.3. Tree construction

The whole 3D centerline, $\mathcal{C}$, is obtained joining all the branches: $\mathcal{C} = \cup_{j=1}^{M} \mathbf{q}_j$. Here, a correct estimation of the bifurcations is needed to assure a correct topology of the 3D centerline. The branches estimation described above is performed independently for each segment, therefore, every bifurcation location is estimated three times, (one for each branch touching it). This can lead to small differences of the bifurcation location estimated for each branch, due to motion or overlapping. To solve this, the bifurcations locations obtained independently are projected to the ray $\overline{\mathbf{b}^l_{n,j}\mathbf{f}_n}$, and then averaged, where $\mathbf{b}^l_{n,j}$ is the bifurcation of branch j at level l at $\mathcal{P}_n$. The level l can have two values (0: proximal or 1: distal), to uniquely identify the two possible bifurcations of a branch. Finally, the branch points are corrected accordingly near the bifurcation point, restricted to the position of their ray bundles $\mathbf{R}_{n,j}$. This process is repeated for each time instant of the cardiac cycle to obtain a 3D+t sequence.

2.4. Radius computation

In the final step, the radius at each 3D point, $\mathbf{q}^i_j$ is obtained mapping back the radius computed at corresponding projection point $\mathbf{p}^i_{n,j}$, and weighted by the aperture effect of the cone beam. If $r_{2D}(\mathbf{p}^i_{n,j})$ is the radius value at $\mathcal{P}_n$, then, this value is assigned to $\mathbf{q}^i_j$ as:

$$r_{3D}(\mathbf{q}^i_j) = r_{2D}(\mathbf{p}^i_{n,j}) \cdot d(\mathbf{f}_n, \mathbf{q}^i_j)/d(\mathbf{f}_n, \mathbf{p}^i_{n,j}).$$

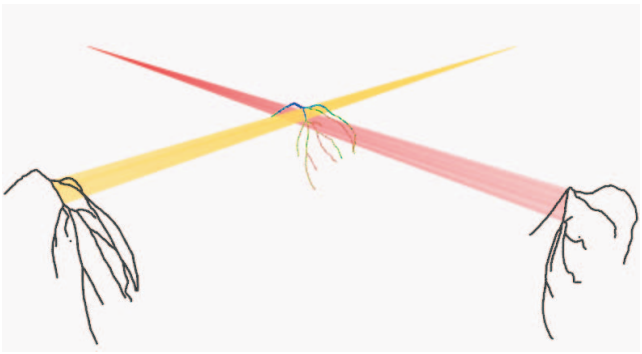


Fig. 3. Ray bundles used to obtain one of the branches from two projections

This step assumes circular cross section of the arteries, which is not true in general. A more realistic approach, using information from more projections, has to be employed in the future to obtain more accurate vessel models.

3. EXPERIMENTS AND RESULTS

3.1. Digital phantom

A digital vascular phantom and 14 forward projections from it, were generated using the same focal and isocenter distances used in the real data sets. The first projection, $\mathcal{P}_0$, was generated at an arbitrary direction, and the rest at angles from $10°$ to $70°$, from $\mathcal{P}_0$ at steps of $5°$. Then, 13 reconstructions were computed using pair of projections: $(\mathcal{P}_0, \mathcal{P}_k), k \in \{1, ..., 13\}$. Fig. 4 (a) shows the phantom and a reconstructed volume using projections separated by $45°$, and in Fig. 4 (d) the reconstructed centerline can be seen (red points) and can be compared with the true centerline (green points). In Fig. 4 (e),(f), the actual projections used for the reconstruction are shown, and the corresponding projections generated from the $45°$ reconstructed volume can be seen in Fig. 4 (b),(c) for comparison.

Quantitative results have been carried out on the 13 volumes to study the angle influence in the reconstruction. In Fig. 5 (left), the average and standard deviation of the minimum distances between the reconstructed centerline points $\mathcal{C}_r$ with respect to the true centerline points $\mathcal{C}_t$ is shown. The minimum distance for each point $\mathbf{p}$ in $\mathcal{C}_r$ is computed as $d_{min}(\mathbf{p}) = min(d(\mathbf{p}, \mathcal{C}_t))$. Numerical results for volume reconstructions, taking into account the vessel radii, are presented in Fig. 5 (right). There, the Jaccard (JC) index (in red) and the Dice Similarity (DS) index (in blue) were computed between the phantom and the reconstructed volumes. From both experiments it follows that the error converges for projection angle differences higher than $30°$, and the reconstruction in this phantom is therefore good, with JC values up to 0.72, DS values up to 0.83 and minimum average centerline distance discrepancies around 0.51 mm. The main errors are found near bifurcation and end points.

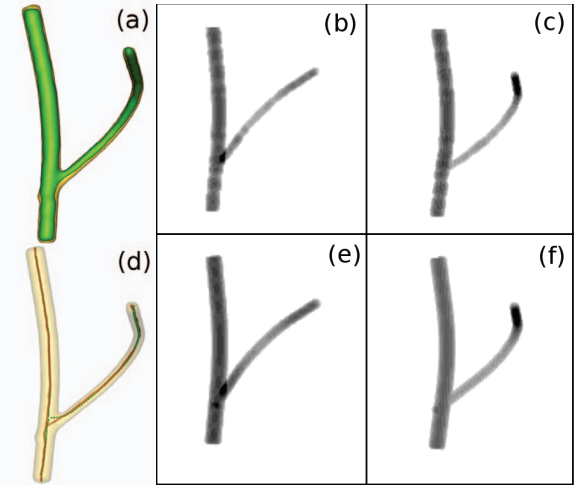


Fig. 4. (a): phantom surface (yellow) and reconstructed volume (green); (d): phantom surface, true centerline points (green points) and reconstructed centerline points (red); (e-f): phantom projections used for the reconstruction; (b-c): corresponding projections of the reconstructed volume.

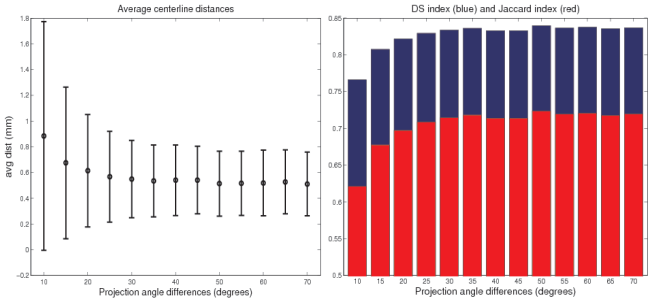


Fig. 5. Variation of the centerline deviation with respect to the ground truth (left) and JC and DS indices between the reconstructed volumes and the ground truth (right), with the projections angle difference.

3.2. Real data

Fig. 6 (left) shows four reconstructions from the left coronary arteries of a patient data set, corresponding to four different cardiac phases. Fig. 6 (right) shows one model from a different view reconstructed from two projections separated by $64.46°$. The vessels are color coded based on the radius value.

4. CONCLUSIONS

In this paper we have presented a method for the 3D reconstruction of coronary arteries from 3DCA, using correspondences between centerline branches and performing a bundle ray matching to find the best 3D trajectories of the vessels. The results presented here show good accuracy for a static phantom, and correct topological reconstructions in real image sequences, showing that the method is able to account for cardiac motion on different cardiac phases. Although this is a preliminary study in a small set of real data, showing good performance, further validation should be made in a bigger number of data sets.

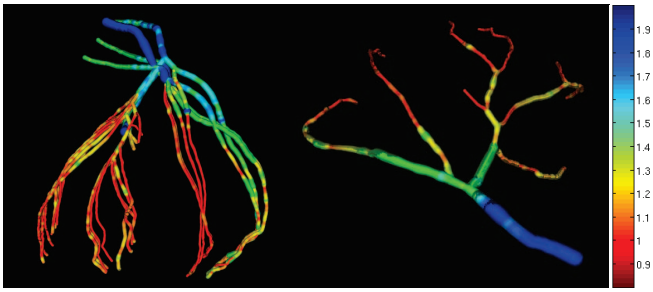


Fig. 6. Coronary artery model reconstructed from real patient data. Left: reconstructed models at four cardiac phases, right: top view of one reconstruction.

5. REFERENCES

[1] A. Arbab-Zadeh, J. Texter, and K. Ostbye, "Quantification of lumen stenoses with known dimensions by conventional angiography and CT? implications for the use of angiography as a gold standard," *Heart*, vol. 96, pp. 1358–1363, 2010.

[2] C. Blondel, G. Malandain, R. Vaillant, and N. Ayache, "Reconstruction of coronary arteries from a single rotational X-ray projection sequence," *Trans. Med. Imaging.*, vol. 25, no. 5, pp. 653–663, 2006.

[3] E. Hansis, D. Schafer, O. Dossel, , and M. Grass, "Evaluation of iterative sparse object reconstruction from few projections for 3-D rotational coronary angiography," *Trans. Med. Imaging.*, vol. 27, no. 11, pp. 1548–1555, 2008.

[4] M. Li, H. Kudo, J. Hu, and R. H. Johnson, "Improved iterative algorithm for sparse object reconstruction and its performance evaluation with micro-CT data," *IEEE Trans. Nucl. Sci.*, vol. 51, no. 3, pp. 659–666, 2004.

[5] U. Jandt, D. Schfer, M. Grass, and V. Rasche, "Automatic generation of 3D coronary artery centerlines using rotational X-ray angiography," *Med. Imag. Anal.*, vol. 13, no. 6, pp. 846–858, 2009.

[6] J. Yang, Y. Wang, Y. Liu, S. Tang, and W. Chen, "Novel approach for 3-D reconstruction of coronary arteries from 2 uncalibrated angiographic images," *Trans. image. processing.*, vol. 18, no. 7, pp. 1563–1572, 2009.

[7] A.F. Frangi, W.J. Niessen, and M.A. Viergever K.L. Vincken, "Multiscale vessel enhancement filtering," in *W.M. Wells, A. Colchester and S.L. Delp (eds.), MICCAI'98, LNCS, Berlin, Germany*, 1998, vol. 1496, pp. 130–137.